

Article

CFD Modeling of a Stirred Anaerobic Digestion Tank for Evaluating Energy Consumption Through Mixing

Soroush Dabiri ^{1,*}, Alireza Noorpoor ², Maziar Arfaee ³, Prashant Kumar ¹ and Wolfgang Rauch ¹

¹ Unit of Environmental Engineering, University of Innsbruck, 6020 Innsbruck, Austria; prashant.kumar@uibk.ac.at (P.K.); wolfgang.rauch@uibk.ac.at (W.R.)

² School of Environment, College of Engineering, University of Tehran, Tehran 13145-1384, Iran; noorpoor@ut.ac.ir

³ Amsterdam UMC, 41883 Amsterdam, The Netherlands; m.arfaee@amsterdamumc.nl

* Correspondence: author: soroush.dabiri@uibk.ac.at, Tel.: +43-512-507-62104

Abstract: The anaerobic digestion process is an effective means to eliminate the detrimental impacts of cattle manure discharge into the environment, i.e., biochemical contamination and substantial methane emissions, the latter leading to global warming. For proper operation of anaerobic digesters, an efficient mixing provides a relatively homogenous mixture of the feedstock within the tank. This study aims to investigate the mixing process and the total energy consumption needed for stirring by using an asymmetrical mixer. A further objective is to analyze the formation of stagnant volume and the velocity gradient in the digester in order to assure the mixing efficiency of the mixer type. The computational model is implemented as the finite volume method, and the rheological properties of the feedstock are considered. The results are validated by comparing the on-site power consumption of the mixer with the values obtained by the numerical torque. At various mixer speeds, the dead volume does not exceed 0.5% of the digester tank; however, with the increase of the mixer rotation speed, the energy consumption of the mixer increases drastically.

Keywords: anaerobic digestion; computational fluid dynamics; dead volume; rheological fluid; stirred tank

Citation: Dabiri, S.; Noorpoor, A.; Arfaee, M.; Kumar, P.; Rauch, W. CFD Modeling of a Stirred Anaerobic Digestion Tank for Evaluating Energy Consumption Through Mixing. *Water* **2021**, *13*, 1629. <https://doi.org/10.3390/w13121629>

Academic Editors: Jacek Mąkinia and Yongmei Li

Received: 15 April 2021

Accepted: 7 June 2021

Published: 9 June 2021

Publisher's Note: MDPI stays neutral with regard to jurisdictional claims in published maps and institutional affiliations.



Copyright: © 2021 by the authors. Licensee MDPI, Basel, Switzerland. This article is an open access article distributed under the terms and conditions of the Creative Commons Attribution (CC BY) license (<http://creativecommons.org/licenses/by/4.0/>).

1. Introduction

Due to the release of greenhouse gases to the atmosphere, global warming has been the main environmental challenge in the past decades. The international panel on climate change has demonstrated that—over a period of 100 years—the standard global warming potential of methane emissions amounts to 25 times that of carbon dioxide emissions [1]. However, since methane is the main part of the biogas generated by anaerobic digestion (AD), the release impacts must hence be alleviated.

AD is a process where organic matter is decomposed synergistically by a microbial consortium in the absence of oxygen [2]. The inlet feed of AD, known as feedstock, can be a wide range of organic materials, which tend to consist of waste materials such as animal manure [3], municipal sludge [4], industrial organic waste [5], and agricultural residues [6]. As described in [7], livestock activities often produce large amounts of manure, which affect soil, water, and air quality through contamination, gas emissions, and nutrient leaching if released directly to the environment [8]. Not only do AD tanks ameliorate the impacts of livestock manure (by minimizing/eliminating the detrimental aspects of microorganisms, such as antibiotic-resistant genes, oxytetracycline, and metabolites [9]), but they also produce fertilizers and biogas from the initial sludge simultaneously [10].

In order to evaluate the behavior of the feedstock within the digester, what is needed is to model the digester and simulate various aspects of the process. Among various physical aspects of the process, the quality of mixing is a significant factor to obtain optimum

process conditions for growing anaerobic micro-organisms [11], while ineffective mixing leads to various problems such as stratification and short-circuiting in the digester, as well as variation of pH and temperature [12] and the formation of surface crusts. It is evident that the higher the active volume, the more efficient is the mixing. Accordingly, the efficiency of mixing can be determined by calculating the inactive volume, also known as dead zones, and the velocity gradient [13]. This helps operators to analyze the type and performance of mixing so that the agitating feedstock approaches an ideally mixed condition with minimum dead zones [14].

Computational fluid dynamics (CFD) is a numerical method to predict the hydrodynamics of fluid flows in bioreactors, thus allowing estimation of the mixing quality within the AD tanks [15]. The finite volume method (FVM) [16], as one of the most robust CFD approaches, is employed in the current study to estimate the hydrodynamics. To analyze the mixing quality of the feedstock inside the AD tank, various studies have been carried out. Some papers have suggested using the mean value of the fluid viscosity for CFD modeling of the mixing in bioreactors [17]; however, some others claim that the non-Newtonian properties of the sludge are important in mixing simulations [18,19].

Regarding mixing methods for AD tanks, a number of research studies are found in the literature. Zhang et al. [20] compared the flow field and power consumption in the digesters with different feedstock materials, utilizing CFD. They employed the standard $k - \epsilon$ turbulence model to simulate the tank stirred by an impeller and validated the numerical results with experimental data. Bridgeman [21] demonstrated the ability of CFD for modeling agitation in bioreactors, utilizing an impeller to agitate the AD tank. He also considered the non-Newtonian behavior of the feedstock and validated his results by comparing the numerical value for the power consumption of the mixer derived from a function of energy dissipation rate with that obtained by experimental data.

To agitate the feedstock inside the digester, gas injection and also fluid recirculation systems are utilized in some cases [22]. Dapelo et al. [23] presented an innovative Euler-Lagrangian approach in CFD for simulating the fluid flow of an AD tank which utilizes gas injection as mixer. They assessed the accuracy of their results by visualization of the flow field in a lab-scale model with particle image velocimetry (PIV).

Sajjadi et al. [4] modeled an AD reactor which uses fluid injectors to recirculate the feedstock. They showed the importance of the location of both the inlet and outlet fluid jets. López-Jiménez et al. [24] simulated the process of mixing in an AD tank in which the sludge was recycled into the tank at high velocities. They modeled the pump inlets with different entrance angles and nozzle shapes to accelerate the inlet velocity. Reynolds-averaged Navier-Stokes (RANS) equations were solved in a single-phase CFD model considering both Newtonian and non-Newtonian characteristics for the sludge.

Since the injection approaches require prepared equipment, in some cases it is not easy to utilize them. This is why impellers are installed more frequently. There are also other methods for ensuring agitation in digesters, e.g., draft-tube mixers [25,26]. In some cases, the agitation is caused just by the inlet flow recirculation depending on the geometry [27]. Hernández-Aguilar et al. [28] solved the CFD equations to evaluate different recirculation configurations while considering the rheological properties of the fluid for an egg-shaped digester without a mixer. Instead, the feedstock was agitated by flow recirculation only. Based on the Reynolds number, they used a laminar flow model. Finally, they showed velocity profiles in three different feed and drain configurations and distinguished the optimum fluid agitation between the designed models. According to the aforementioned articles, CFD is a desirable approach to predict the behavior of fluid within the AD tanks. Therefore, the efficiency of the digester can be evaluated to avoid the unexpected inhibition of the process.

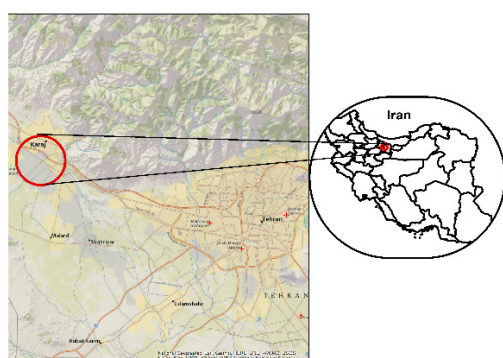
The previous studies on stirred tanks have focused on rotating mixers located at the center of the tank, but the mixing quality (i.e., dead volume, mixing time, velocity gradient, etc.) of the asymmetrical mixers is largely unknown. Consequently, in this study, the mixing quality is extensively investigated for a mixer that is located asymmetrically at one

side of the tank. Moreover, since the energy consumption of the mixer has a significant effect on the total energy efficiency of digesters, there is a need to get insight into the mixer energy consumption and its relation to the mixing efficiency. The current study aims at evaluating the mixer energy consumption, in addition to dead volume and velocity gradient, for assuring mixing efficiency. TS concentration and the subsequent non-Newtonian characteristics as well as the mixer rotation speed are the significant factors, whose effects on the mixing efficiency are studied. After designing the geometry of the model, including the effective components on the mixing quality, a mesh is implemented. Next, to determine the amount of dead volume and the relation of mixer velocities and energy consumption, velocity and pressure fields are obtained through solving fluid flow equations, based on the SIMPLE algorithm, considering the non-Newtonian characteristics of the fluid.

2. Materials and Methods

2.1. Geometry and Meshing

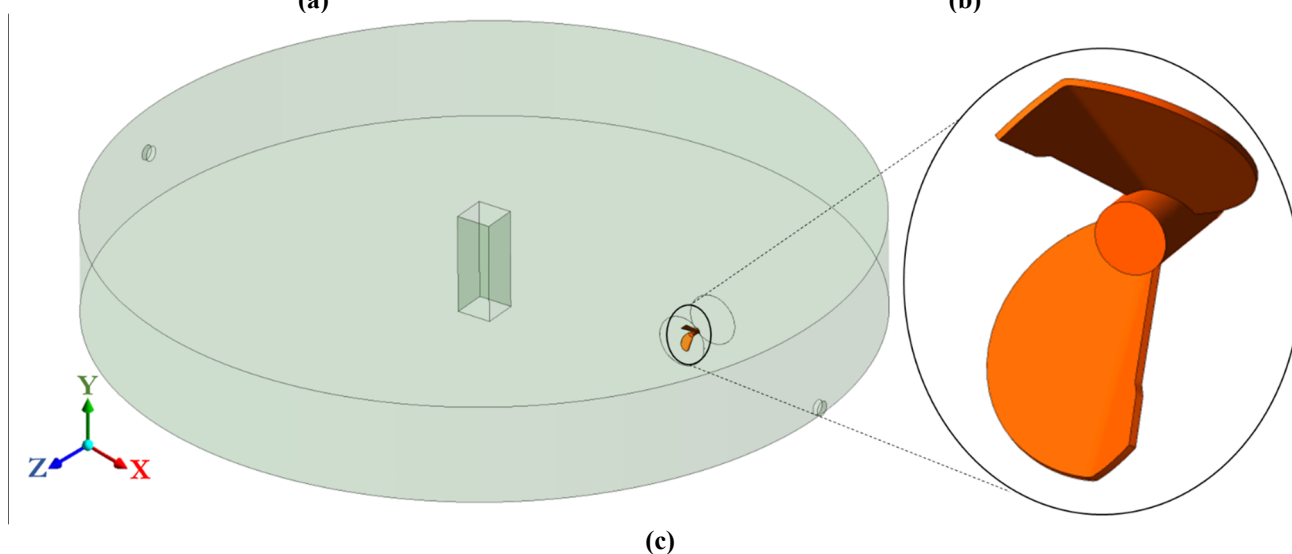
In this study, a full-scale simulation is conducted according to the properties of the real AD in Malaard Livestock Yard located 70 km west of Tehran, Iran. It is a cylindrical tank whose external and internal views are displayed in Figure 1(a). The tank is 15 m in diameter, and its height is 3 m with the wet height being 2 m. For supporting the base of the roof, there is a vertical square column with a 0.7 m edge at the center of the tank. Figure 1(b) shows an internal view of the digester tank.



(a)



(b)



(c)

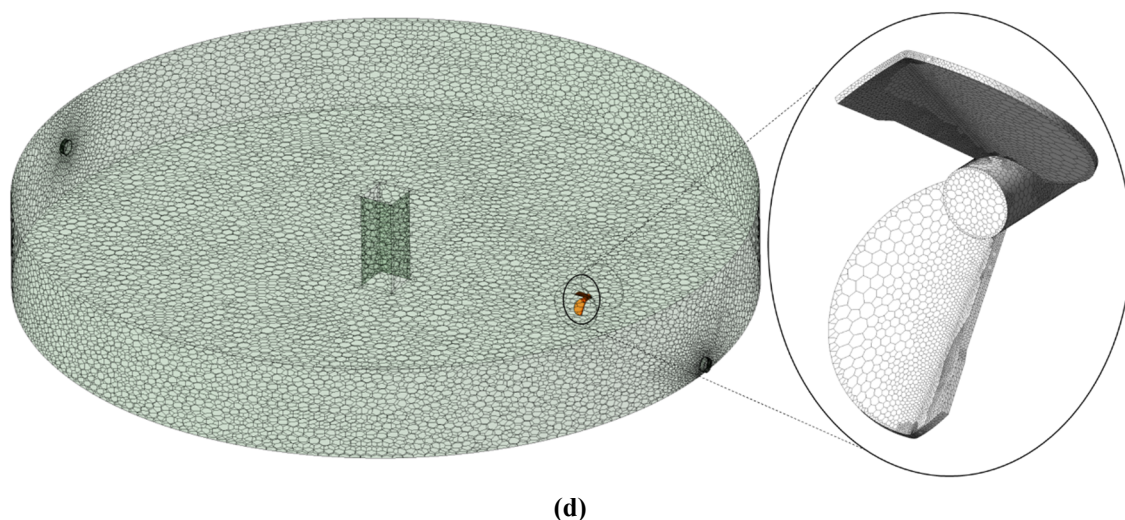


Figure 1. The location of the digester tank (a), the internal view of digester tank including its mixer (b), designed geometry to simulate agitation inside the tank (c), mesh implementation for the tank and mixer zones (d).

The inlet and outlet tubes are 0.2 m in diameter and located at the height of 0.2 and 1.0 m from the base, respectively. The feedstock is agitated utilizing a submersible rotating mixer [29], whose impeller is designed and incorporated within the mesh geometry. Each blade of the impeller is 0.36 m in its maximum extension, and the diameter of the central shaft is 0.10 m. Figure 1(c) illustrates the designed mixer, which is located at the height of 1 m and with the distance of 4.8 m from the center of the tank.

The built-in ANSYS meshing tool is used to mesh the whole geometry of the AD tank. For improving mesh quality around the blades of the mixer, mesh cell sizes are inflated smoothly. In order to conduct a continuous growth of the tetrahedral elements at the boundaries of the domain, the layers of boundary meshes with a growth rate of 1.2 are applied. After mesh refinement, the final network cells are converted to polyhedral cells with the number of elements being 222,058. Figure 1(d) shows the view of the implemented mesh of the tank zone, as well as the implemented mesh of the blades of the mixer zone.

2.2. Assumptions

- Since the flow enters the digester for just 15 min during a six-hour period, the effect of the inlet and outlet flow is not significant.
- 2 m of the tank is filled by the feedstock.
- The shear-thinning non-Newtonian characteristics of the feedstock are considered.
- The density of the fluid is constant and calculated as 1001.7 kg/m^3 , based on [30].
- The effect of temperature is assumed as constant.

2.3. CFD Method

In order to compute the fluid dynamics within the feedstock of the AD, the governing equations of mass and momentum conservation are solved in both the transient and steady state for an incompressible fluid, using ANSYS Fluent v19.2 software [16].

For the flow regime inside the digester, the generalized Reynolds number was calculated as described in [31]. Accordingly, the flow regime is identified as turbulent, as the calculated Reynolds number exceeds 20,000 [30]. Since previous studies (such as [32] and [33]), have proved the robustness of the RNG $k - \varepsilon$ turbulence model to predict bioreactors hydrodynamics with minimal computational effort, we have also obtained the turbulent closure by the RNG $k - \varepsilon$ model [34]. In addition, the scalable wall functions option is activated to improve the accuracy of the $k - \varepsilon$ model for calculating the equations close to the walls [35]. The solver is pressure-based, and the SIMPLE algorithm is employed to

solve the flow equations in a second-order upwind discretization scheme. In addition, the under-relaxation factors are aligned as default, and no limitations for the magnitude of the residuals is defined until the convergence would be achieved.

2.4. Equations

The mass and momentum equations are solved to predict the formation of pressure and velocity fields. Equation (1) is the continuity and Equation (2) is the conservation of momentum for incompressible flows in a Cartesian coordinate system [36].

$$\frac{\partial \rho}{\partial t} + \nabla(\rho \vec{V}) = 0 \quad (1)$$

where ρ is the density, \vec{V} is the velocity of the fluid in the control volume.

$$\frac{\partial(\rho \vec{V})}{\partial t} + \nabla(\rho \vec{V} \vec{V}) = -\nabla p + \nabla(\bar{\tau}) + \rho \vec{g} \quad (2)$$

where p is the static pressure and $\bar{\tau}$ is the viscous stress tensor.

The RNG $k - \varepsilon$ model consists of two transport equations for two parameters, turbulent kinetic energy (k) and the energy dissipation rate (ε) [34].

The rotation of the impeller is simulated using the multiple reference frame (MRF) approach, and the equations in the moving reference frame can be found in [16].

2.5. Physical Characteristics

The concentration of total solids (TS) loading is an effective parameter on non-Newtonian behavior of the feedstock. The mixing mode is continuous. The fluid flow within the plant is cattle manure feedstock, with a TS concentration equal to about 120,500 ppm, or almost 12.1%. Thus, the non-Newtonian power-law model is activated to calculate the viscosity of the fluid. It should be noted that the power-law model cannot support scenarios with infinite viscosities. Thus, other alternative methods, such as the Herschel-Bulkey model, are used by some researchers [18]. However, according to literature references [26,30,37] the power-law method is capable of estimating the sludge behavior up to a TS concentration of 12%. Therefore, the power-law model is also applied in this study, due to its low computational complexity. At the mesophilic temperature of 35 °C the non-Newtonian pseudo-plastic (shear-thinning) properties of the sludge are based on [26] and [38], depicted by Table 1.

Table 1. Rheological properties used for sludge modeling (from [38]).

TS (%)	K ($Pa\ s^n$)	n	$\dot{\gamma}$ (s^{-1})	η_{min} ($Pa\ s$)	η_{max} ($Pa\ s$)
12.1	5.885	0.367	3–149	0.25	2.93

The apparent viscosity (η) of the rheological fluid depends on shear rate ($\dot{\gamma}$). Using a power-law equation, the viscosity is described by:

$$\eta = K(\dot{\gamma})^{n-1} \quad (3)$$

where η denotes apparent viscosity, $\dot{\gamma}$ is the shear rate, K represents the consistency index, and n indicates the flow behavior index, which should be below one for pseudo-plastic fluids.

2.6. Boundary and Zone Conditions

The boundary condition imposed to the digester is a no-slip shear condition on the walls. The upper surface of the model is assumed as wall due to the aggregation of the sludge. Thus, the feedstock is trapped between the upper, lower, and lateral walls, as well as the walls of central column. The applied boundary conditions are listed in Table 2.

Table 2. The boundary conditions of the model.

Boundary	Type	Characteristic
Lateral walls	Wall	No-slip shear condition
Mixer impellers		
Central column walls		
Upper surface		
Lower surface		

Two zones are created for the simulation. The tank zone is the total volume of the tank and the mixer zone is the rotating zone in the vicinity of the impeller. The rotating region (including the mixer) is 1 m in diameter and rotates at the speed of 300 rpm.

3. Results and Discussion

3.1. Validation

As shown by Bridgeman [21], model validation can be carried out by comparing the real power consumption (P) of the mixer with that obtained from the numerical simulation. Empirical power input measurements are determined from applied torque measured by a torque transducer. Thus, the power consumption is:

$$P = 2\pi\omega T \quad (4)$$

Where ω represents the rotating speed and T is the applied torque.

In the numerical simulation, the torque imposed on the impellers is calculated through the post-processing tools of the software, by summing the cross products of the pressure and viscous force vectors with the moment vector (the vector from the specified moment center to the force origin) for each face. It is also noteworthy to mention that we neglect additional (and unknown) power losses induced by gear boxes and the like. The on-site power consumption of the mixer is 18.1 kW while the obtained power consumption from the simulation is equal to 24.5 kW, which differs by about 26% from the real value for power consumption. This difference can, e.g., be due to uncertainties in the estimation of rheological characteristics. However, the difference is acceptable, based on the difference ranges calculated in [21]. Another method also exists for calculating the power consumption, which is based on the energy dissipation rate. In this method, the overall power consumption is estimated by integrating the local power consumption numerically over the entire volume of the tank, so the power consumption of the mixer is calculated via:

$$P = \rho \int \varepsilon dV \quad (5)$$

where ρ is the density, ε denotes energy dissipation rate, and V indicates the volume. The obtained numerical power consumption based on this method is equal to 22.3 kW (around 9% lower than the one obtained via surface integrals and differing by about 23.4% from the real value for power consumption). Although the calculated power consumption via the energy dissipation rate is closer to the on-site data, this method is not seen as accurate as calculating the numerical torque [39]. Thus, we apply the numerical torque methods for the remainder of the simulations.

3.2. Grid Independence

To evaluate the mesh independence, three different sizes for the elements are analyzed based on [40] and [18]. Consequently, a series of simulations are conducted, in which the numbers of elements are chosen as 101,894, 222,058, and 462,912. For each simulation, the velocity profile at the vertical line, crossing a specific point (located with a 90-degree angular distance from the mixer, and at the same radial distance as the mixer), was computed for each mesh structure, and then the results were compared to each other,

according to [26]. Figure 2 depicts the velocity profile along the mentioned vertical line for the three mesh networks.

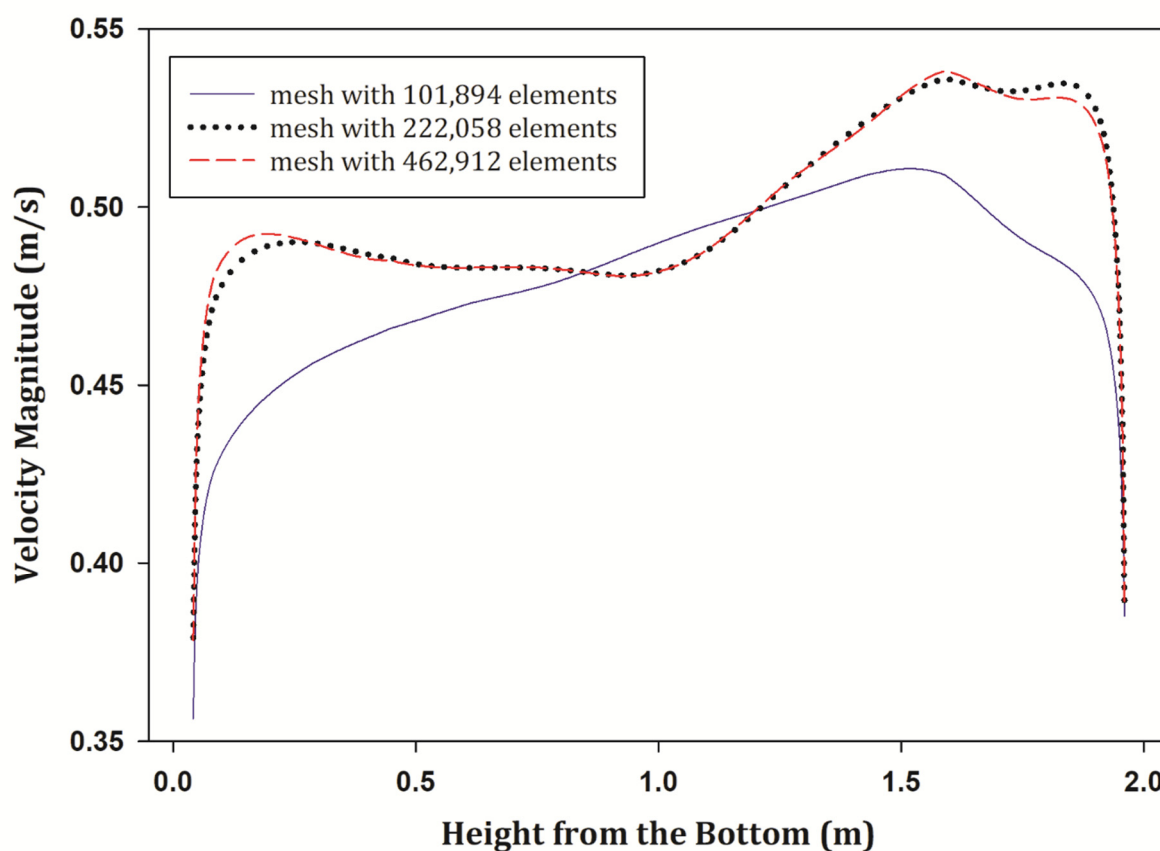


Figure 2. Velocity profiles along the vertical line within the digester for the meshes with 101,894, 222,058, and 462,912 elements.

It was observed that the value for the velocity magnitude in the model with 101,894 elements differed more than 5.3% from that obtained by the model containing 222,058 elements, while the data of the model with 222,058 elements differed only about 0.5% compared to the model with 462,912 elements. Therefore, the velocity profiles for the models with 222,058 and 462,912 elements were in a very good agreement. In addition, based on the method in [40], the amount of the grid convergence index (GCI) was calculated for the central point of the obtained velocity profile. The variables φ_1 , φ_2 , and φ_3 denote the velocity magnitude at the mentioned point for the cases with 101,894, 222,058, and 462,912 elements, respectively (see Table 3). The variable φ_{ij} abbreviates $\varphi_j - \varphi_i$, and the ratios of the grid refinement are shown by r_{21} and r_{32} . Then the order of convergence (p) is determined by iteratively solving the 11th equation in [26]. By calculating the relative error between the two finest meshes ($e_{32} = |\frac{\varphi_{32}}{\varphi_2}|$), the GCI value, with a safety factor of 1.25, is calculated as almost equal to 0.02%. It was, thus, concluded that the model with 222,058 elements is suitable for the simulation.

Table 3. The calculated parameters for assessing mesh sensitivity.

Parameter	Unit	Value
φ_1		0.4907
φ_2	m/s	0.4846
φ_3		0.4839
$ \varphi_{21} $	m/s	0.0061

$ \varphi_{32} $		0.0007
r_{21}	-	≈ 1.3
r_{32}	-	≈ 1.3
p	-	8.24
e_{32}	%	0.14

3.3. Contours and Vectors

Velocity data of the model are captured from the simulation results. By Figure 3, the variation of the velocity magnitude in the range of 0 to 0.5 m/s is illustrated along two central vertical planes and three horizontal planes located at the heights of 0.5 m, 1 m, and 1.5 m, respectively. Indeed, the flow within the digester tank is mixed by a rotating impeller, which is employed to prepare a uniform distribution of the organic material in all parts of the tank. The streamlines of the fluid are obtained and illustrated in Figure 4. The streamlines are captured from 50 points and started from three planes located horizontally at the height of 0.5 m, 1 m, and 1.5 m.

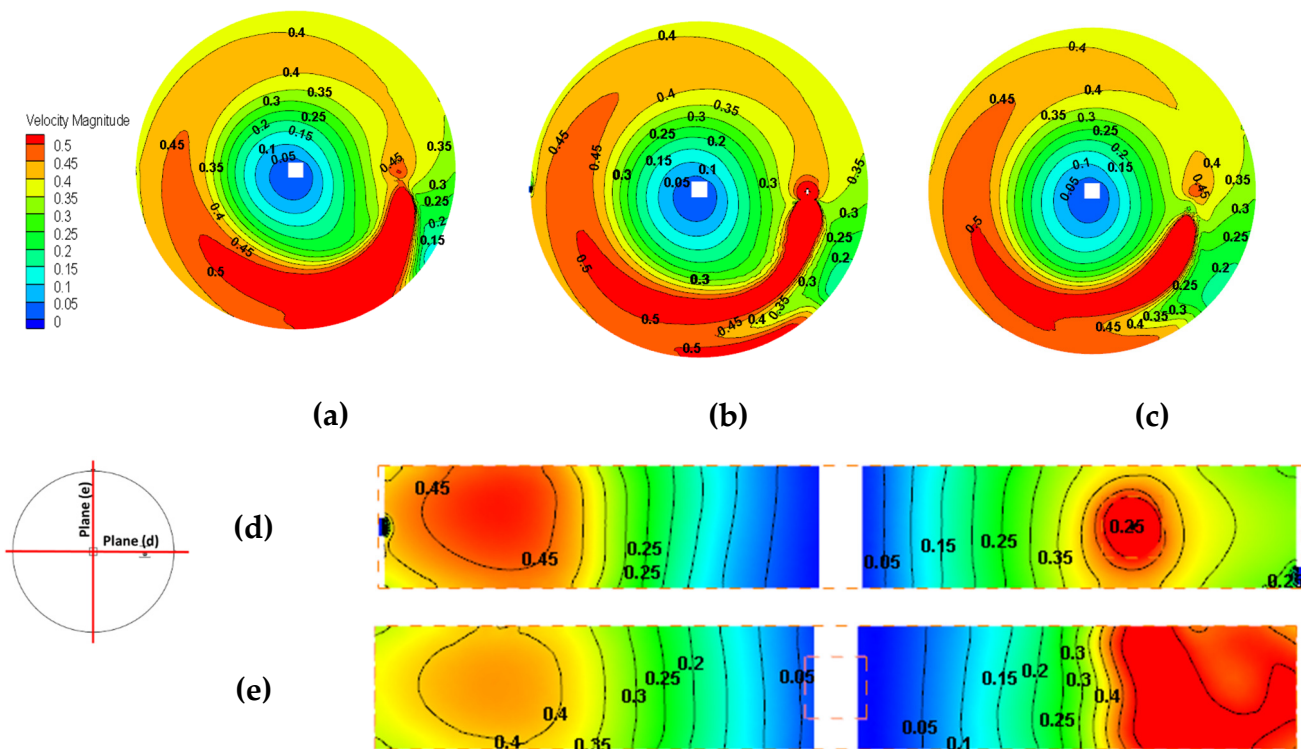


Figure 3. Velocity contours of the three horizontal planes, located at the heights of 0.5 m (a), 1 m (b), and 1.5 m (c) from the floor of the digester; and velocity contours of two vertical planes (d and e) in the digester.

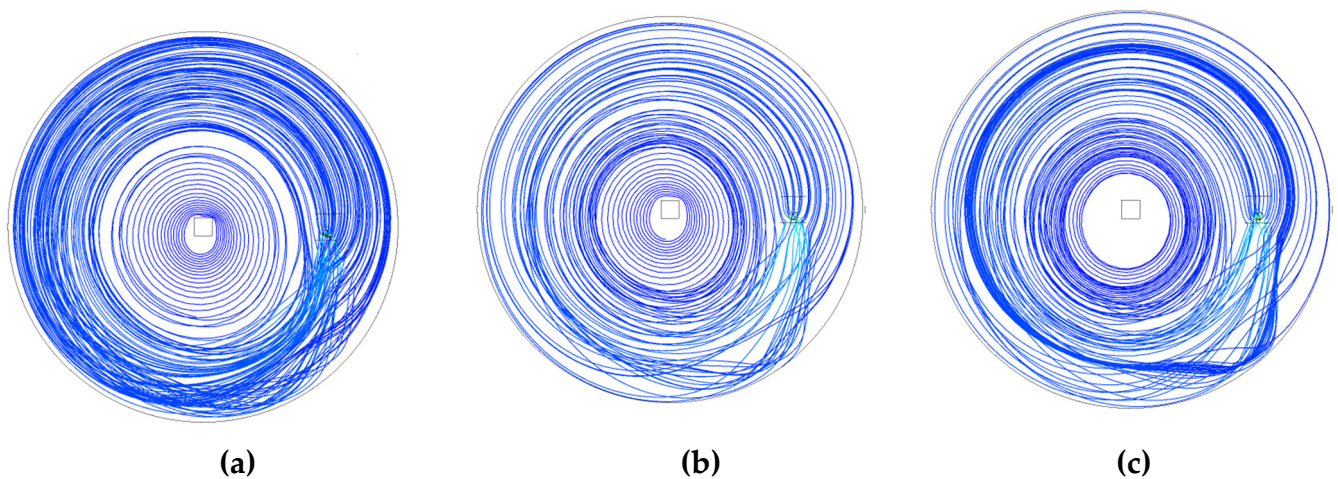


Figure 4. Streamlines derived from three horizontal planes situated at the heights of 0.5 m (a), 1 m (b), and 1.5 m (c) from the floor.

Additionally, for better understanding of the fluid motion, the absolute velocity vectors are presented in Figure 5 in the three horizontal and two vertical planes. The vector map in the horizontal planes, as well as the streamlines in Figure 4, show that the fluid rotates in circular shape and is also agitated well. Likewise, the vector map of the vertical planes illustrates some moving directions which are shaped diagonally. In fact, from these diagonal rotations it is inferred that the material within the AD tank is mixed in an appropriate manner.

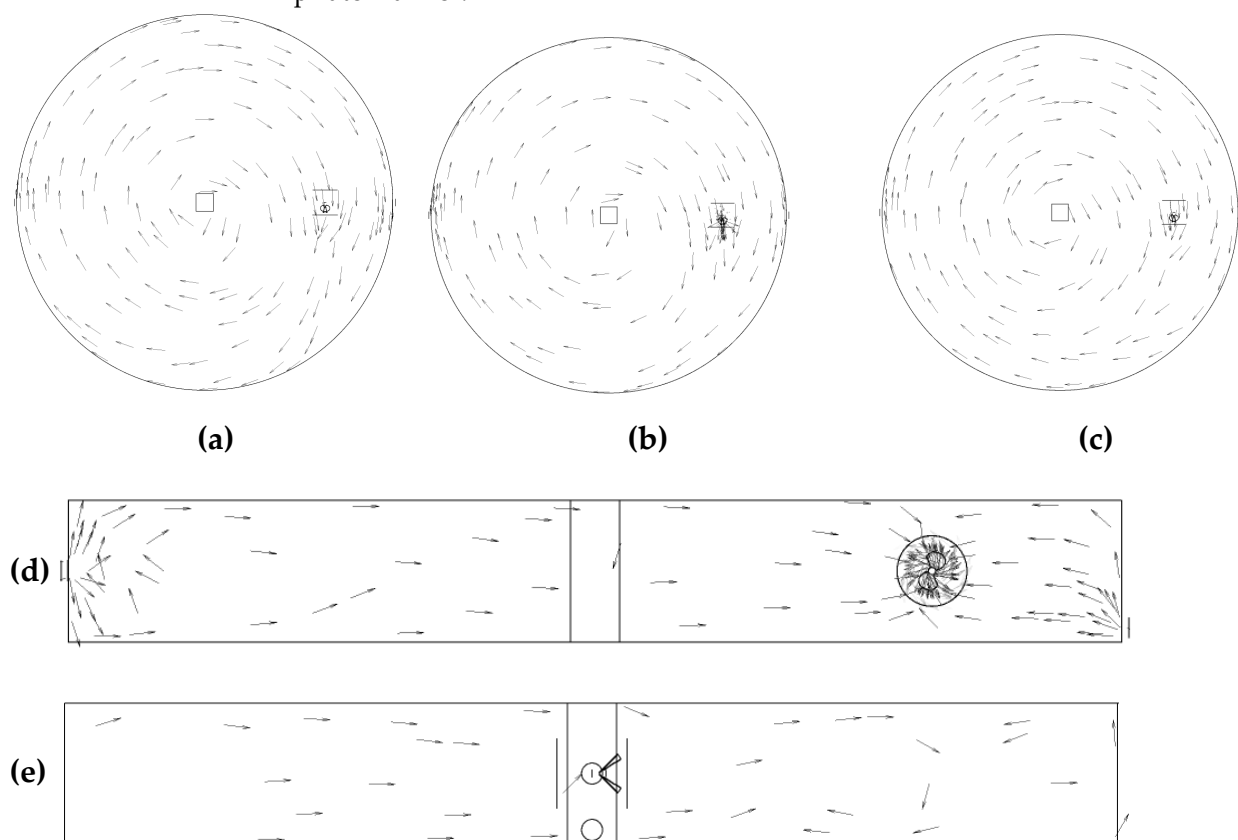


Figure 5. Velocity vectors mapped in the three horizontal planes situated at the heights of 0.5 m (a), 1 m (b), and 1.5 m (c) from the floor, and the two vertical planes located according to Figure 3.

In the current study, the definition of dead zones is chosen according to the definition in [41], where the regions with the sludge velocities less than 5% of the maximum velocity are denoted as dead volume. As in our case, the maximum velocity is between 0.45 and 0.50 m/s (close to the mixer). Therefore, the 0.02 m/s velocity is selected as the threshold for identifying dead volume.

Figure 3 reveals that the velocity magnitude in almost all elements of the tank is above the threshold value of 0.02 m/s. We, hence, conclude that the feedstock within the digester has been agitated properly and the type and the situation of the mixer is appropriate to the evaluated model. As depicted by the velocity contours, the minimum magnitude for velocity is reached even in the vicinity of the central square column. This is due to the no-slip boundary condition of the wall surfaces.

3.4. Data Analysis

For assessing a time-dependent model, it is necessary to carry out a transient simulation and compare its results with the steady-state simulation. After simulation in transient conditions for about 46 min, the corresponding velocity fields are investigated for specified time steps. The velocity magnitude at a specific point (1 m above the bottom and 4.8 m far from the central column) is plotted as a timeline in Figure 6.

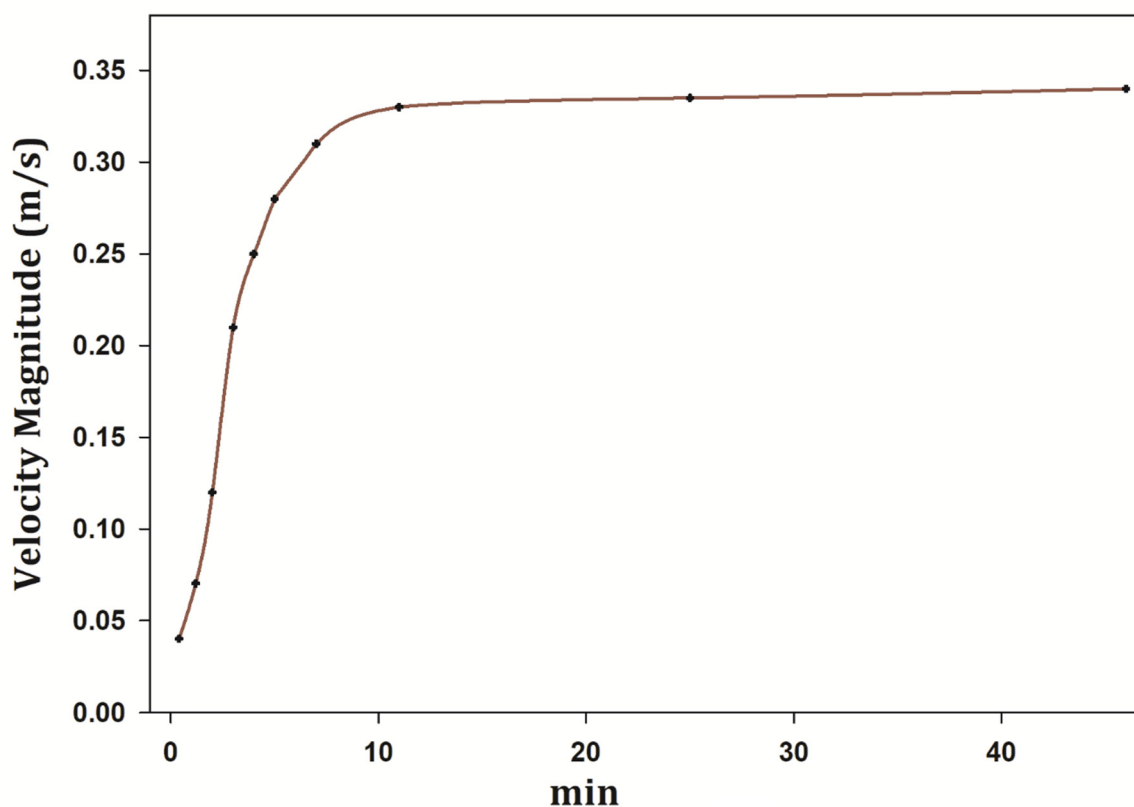


Figure 6. The plot of the velocity magnitude at a specific point over the simulated time.

The velocity magnitude at the probed point increases approx. linear from 0.04 m/s (after 24 sec) to 0.31 m/s (after 7 min). At this point in time, the slope of the timeline declines, reaching 0.33 m/s after 11 min. This is already close to the maximum velocity of 0.36 m/s at the probed point—as derived from the steady-state simulation. As the difference to the steady state value is less than 10%, it can be estimated that the time to reach the steady state at the probe point is 11 min.

In order to investigate the velocity field along with the height of the tank, the average velocities of seven horizontal planes located at heights of 0.25, 0.5, 0.75, 1, 1.25, 1.5, and 1.75 m are computed, and shown by Figure 7.

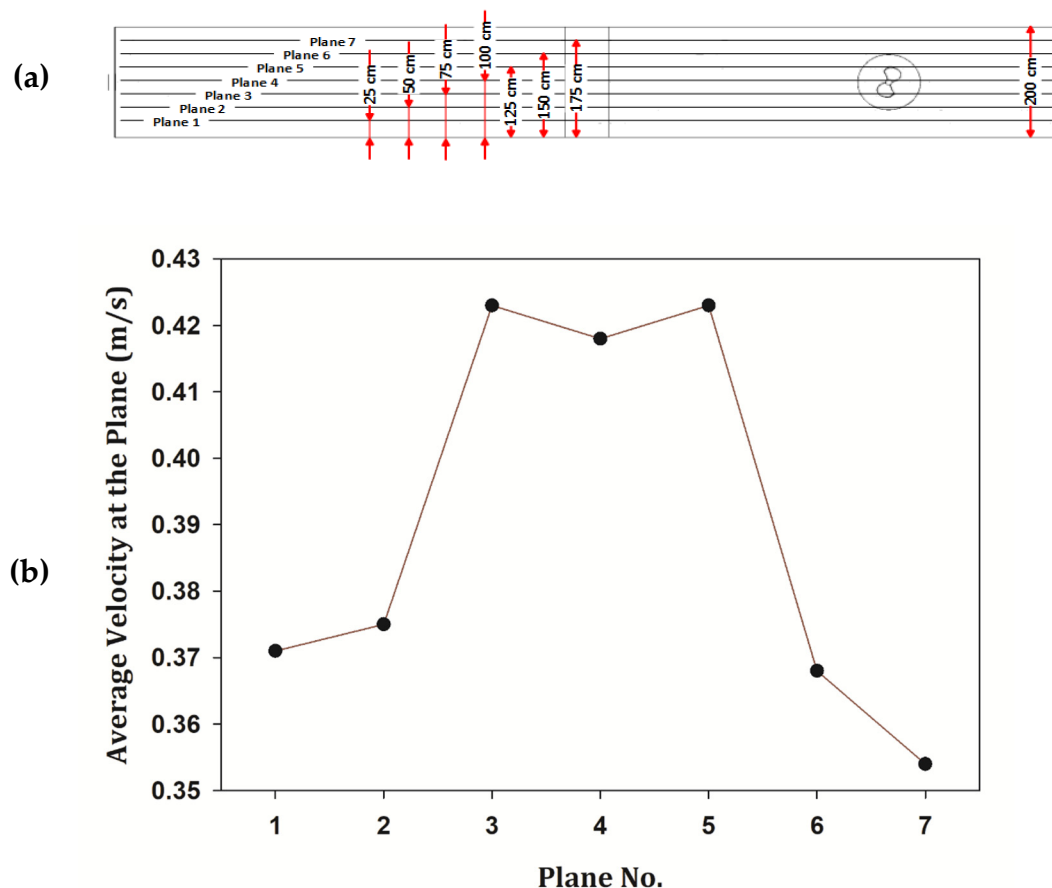


Figure 7. The location of each horizontal plane (a), and the plot of the average velocity at each horizontal plane at its corresponding height (b).

It is observed that the values for averaged velocities stay within the range between 0.35 m/s and 0.43 m/s. The velocities at the central parts of the digester are higher than the ones closer to the bottom and the top surface. This is because of the location of the mixer, which is also at the central height (1 m above the bottom of the tank).

Employing user-defined memory (as declared in [16]), the total volume of the cells with a velocity magnitude below 0.02 m/s (which are considered as stagnant zone) is calculated. For the TS concentration of 12.1%, the stagnant zone value is computed as 1.66 m³ or 0.47% of the volume, respectively.

In order to estimate the effect of the TS concentration on the dead zone volume, the simulation is performed for TS concentrations of 2.5%, 5.4%, 7.5%, and 9.1%, considering individually their specific rheological properties according to [38]. Figure 8 demonstrates that as the TS concentration increases from 2.5 to 12.1 the total value for dead volume also increases from 0.20% (0.71 m³) to 0.47% (1.66 m³), respectively. This shows an increase of about 133%, which can be considered as a significant variation in the total volume of dead zones, although all of the obtained values for the dead volume are negligible as compared to the total volume of the fluid. It is concluded that by increasing the TS concentration, the volume of dead zones increases.

In addition, employing Equation 4, the consumed power by the mixer is estimated for each model with specific TS concentration. The achieved values for the power consumption in the models with different TS concentrations are depicted by Figure 8.

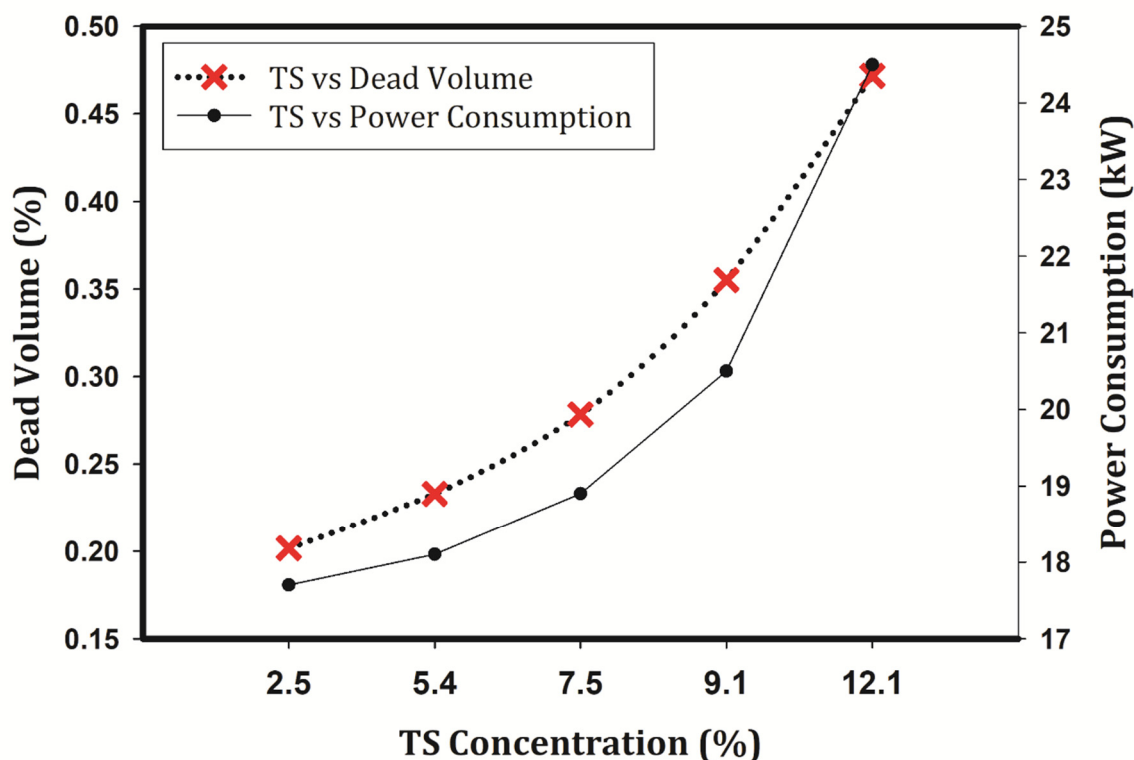


Figure 8. The created dead volume and power consumption for each TS concentration within the feedstock.

It is indicated that by enhancing the TS concentration from 2.5% to 12.1%, the power consumed by the mixer, which is rotating at the constant angular velocity of 300 rpm, increases from 17.7 kW to 24.5 kW. This shows an enhancement of about 27.7% in power consumption. Note that the increase in power consumption is not linear to the increase of TS but rather exponential. This is because of the nonlinear effect to viscous forces for higher TS concentrations.

In many cases, the appropriate agitation has another advantage, i.e., avoiding sedimentation. In order to determine whether the mixing is sufficient to prevent sedimentation of heavy solids in the digester, the velocity gradient is calculated. Calculating the velocity gradient (G) has become a fundamental approach within the water and wastewater industry to classify mixing tanks. According to [42], G can be estimated with local energy dissipation rate:

$$G = \sqrt{\frac{\varepsilon}{\eta}} \quad (6)$$

where ε is the turbulent energy dissipation rate in mass unit and η is the kinematic viscosity.

Sindall et al. [13] have suggested that the velocity gradient should lie between 7.2 and 14.5 s^{-1} . In this research, G is determined by post-processing of the achieved data (utilizing volume integrals in the software) as 26 s^{-1} . Thus, mixing does not avoid formation of the sedimentation layer and an additional sewage pump regime is necessary to improve the performance of the AD. A solution could be reducing the amount of the mixer rotation speed; however, due to structural limitations, reducing the mixing speed is not possible in our case.

In order to investigate a possible prevention of sedimentation, an alternative mixing scenario is tested by situating the mixer 0.25 m lower than its previous location, thus aiming for increased agitation close to the bottom. Subsequently, the mixing quality is analyzed by calculating the dead volume and the velocity gradient. However, for the similar mixing rotation speed of 300 rpm, the dead volume does not decrease but instead increases to 2.60 m³. While this is still only about 0.73% of the digester volume, we denote that the effect is obviously contrary to the intended one (a 36% increase in the amount of dead volume as compared to the case where the mixer is at the central height). For both the velocity gradient and the power consumption, no significant difference is found for this scenario.

Evaluating the effect of mixing speed on the velocity gradient allows one to determine whether it is viable to increase the mixer rotation speed instead of using a sewage pump. The fluid with total solids of 12.1% is analyzed while imposing rotation speed values greater than 300 rpm. Based on the infrastructures, it is considered that the mixer rotates at the angular velocities of 300, 350, 400, 450, and 500 rpm. Similarly, the effect of mixing speed on the dead volume is analyzed. Figure 9 depicts the effects of angular velocity on the dead volume and velocity gradient, respectively.

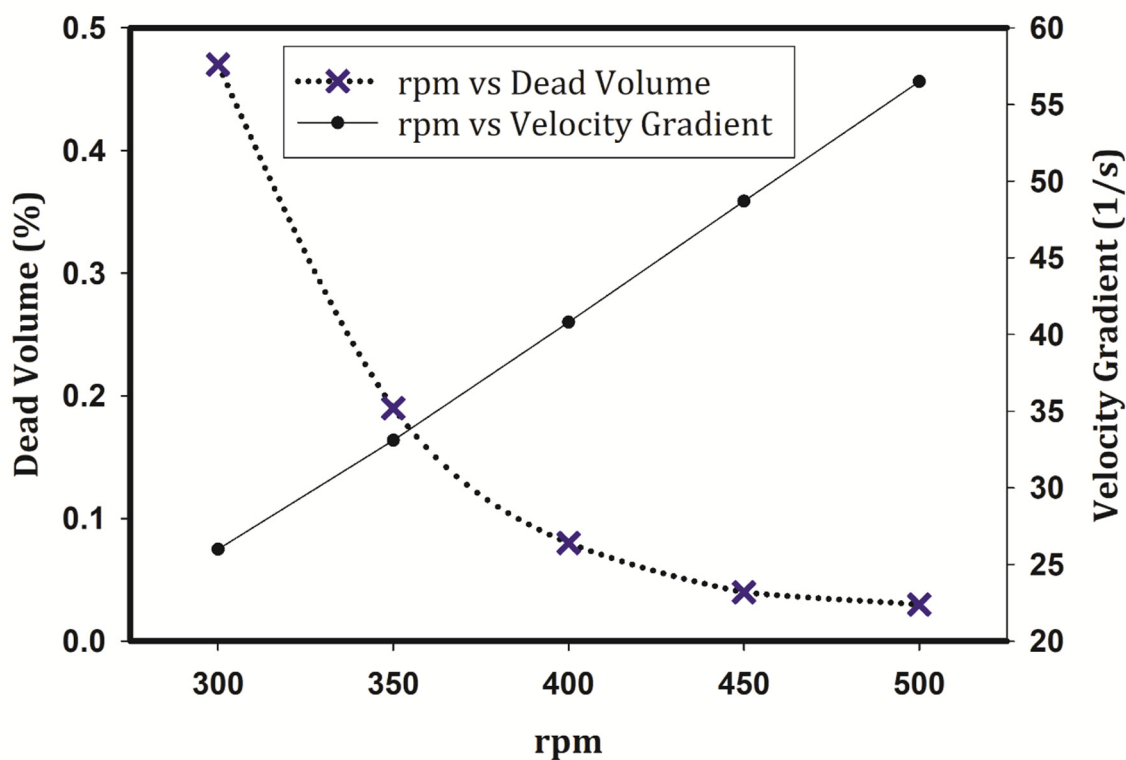


Figure 9. The created dead volume and velocity gradient for each mixer rotation speed.

As to the effect of the mixer rotation speed on the dead volume (Figure 9), it is shown that the values for the dead volume decrease from 1.66 m³ for a rotation speed of 300 rpm to 0.12 m³ for a rotation speed of 500 rpm. In general, the dead volume decreases as the mixer rotation speed increases, but the relation is non-linear. This is different for the velocity gradient as this value increases from 26 s⁻¹ for the mixer with the rotation speed of 300 rpm to 56.5 s⁻¹ for the mixer with the rotation speed of 500 rpm. As the minimum mixer rotation speed (300 rpm) already leads to higher values in velocity gradient, increasing the speed does not help in keeping the G value in its optimum range. Moreover, when the mixer rotates with the speed of 500 rpm, the power consumption increases to about 159.9 kW (according to Equation 5), which is quite high for such a plant size. Indeed, the

amount of power consumption at 500 rpm is more than six times the one required for 300 rpm. For different mixer rotation speeds, the power consumption is summarized in Table 4.

Table 4. The corresponding power consumption for each mixer rotation speed.

Mixer rotation speed (rpm)	Power consumption (kW)
300	24.5
350	47.1
400	78.4
450	117.6
500	159.9

4. Conclusion

The purpose of this study was to evaluate mixing capabilities of an asymmetrical mixer, which rotates at the lateral side of the tank, by employing the CFD method. The energy consumption, mixing time, dead zone, and velocity gradient of the digester tank were analyzed, based on the TS concentration and mixer rotation speed. When the mixer rotation speed was 300 rpm, the dead zone volume amounted to about 0.47% of the total volume of the digester; however, the velocity gradient was higher than the optimum region. The following findings are obtained:

- The dead zone was found near the central column and the walls of the digester because the applied mixer mostly affects the regions located at the same height and radial distance as the mixer.
- Power consumption increases by increasing TS concentrations, especially at higher TS concentrations. Similarly, by increasing TS concentrations, the amount of dead volume increases considerably.
- There is not a huge change for dead volume once the mixer rotation speed increases to 400 rpm and higher, while the energy needed for mixing increases.
- It is not recommended to increase the mixer rotation speed to more than 300 rpm, since—besides the deteriorative effect of the higher velocity gradient—the energy consumption of the mixer increases.

In order to reduce power consumption, another possible scenario is “intermittent mixing”, which has shown good results in terms of biogas production [43]. For future work, it is interesting to focus on such scenarios.

Author Contributions: Conceptualization, A.N. and S.D.; Methodology, A.N., W.R., and S.D.; Software, S.D. and M.A.; Validation, P.K. and S.D.; Resources, W.R.; Writing—original draft preparation, S.D.; Writing—review and editing, W.R. and P.K.; Visualization, S.D.; supervision, W.R. and A.N. All authors have read and agreed to the published version of the manuscript.

Funding: This research was funded by the Federal Ministry of the Republic of Austria for Agriculture, Regions and Tourism in collaboration with the Kommunalkredit Public Consulting GmbH [grant number: B801259].

Institutional Review Board Statement: Not applicable.

Informed Consent Statement: Not applicable.

Data Availability Statement: The data presented in this study is available on request from the corresponding author.

Acknowledgments: We appreciate the support of the environmental research group in the Graduate Faculty of Environment, University of Tehran. We have also benefited from Mr. Sina Hesarkazazi for the geographic map design.

Conflicts of Interest: The authors declare no conflict of interest. The funders had no role in the design of the study; in the collection, analyses, or interpretation of data; in the writing of the manuscript, or in the decision to publish the results.

References

1. Mitsch, W.J.; Bernal, B.; Nahlik, A.M.; Mander, Ü.; Zhang, L.; Anderson, C.J.; Jørgensen, S.E.; Brix, H. Wetlands, carbon, and climate change. *Landsc. Ecol.* **2013**, *28*, 583–597.
2. Bajpai, P. *Anaerobic technology in pulp and paper industry*; Springer: Singapore, 2017.
3. Passos, F.; Ortega, V.; Donoso-Bravo, A. Thermochemical pretreatment and anaerobic digestion of dairy cow manure: Experimental and economic evaluation. *Bioresour. Technol.* **2017**, *227*, 239–246.
4. Sajjadi, B.; Raman, A.A.A.; Parthasarathy, R. Fluid dynamic analysis of non-Newtonian flow behavior of municipal sludge simulant in anaerobic digesters using submerged, recirculating jets. *Chem. Eng. J.* **2016**, *298*, 259–270.
5. Hamawand, I. Anaerobic digestion process and bio-energy in meat industry: A review and a potential. *Renew. Sustain. Energy Rev.* **2015**, *44*, 37–51.
6. Yang, L.; Kopsell, D.E.; Kottke, A.M.; Johnson, M.Q. Development of a cartridge design anaerobic digestion system for lignocellulosic biomass. *Biosyst. Eng.* **2017**, *160*, 134–139.
7. Melse, R.W.; Hol, J.M. Biofiltration of exhaust air from animal houses: Evaluation of removal efficiencies and practical experiences with biobeds at three field sites. *Biosyst. Eng.* **2017**, *159*, 59–69.
8. Guerci, M.; Knudsen, M.T.; Bava, L.; Zucali, M.; Schönbach, P.; Kristensen, T. Parameters affecting the environmental impact of a range of dairy farming systems in Denmark, Germany and Italy. *J. Clean. Prod.* **2013**, *54*, 133–141.
9. Turker, G.; Akyol, Ç.; Ince, O.; Aydin, S.; Ince, B. Operating conditions influence microbial community structures, elimination of the antibiotic resistance genes and metabolites during anaerobic digestion of cow manure in the presence of oxytetracycline. *Ecotoxicol. Environ. Saf.* **2018**, *147*, 349–356.
10. Fodor, Z.; Klemeš, J.J. Waste as alternative fuel—Minimising emissions and effluents by advanced design. *Process Saf. Environ. Prot.* **2012**, *90*, 263–284.
11. Coward, T.; Tribe, H.; Harvey, A.P. Opportunities for process intensification in the UK water industry: A review. *J. Water Process Eng.* **2018**, *21*, 116–126.
12. Rennie, T.J.; Baldé, H.; Gordon, R.J.; Smith, W.N.; VanderZaag, A.C. A 3-D model to predict the temperature of liquid manure within storage tanks. *Biosyst. Eng.* **2017**, *163*, 50–65.
13. Sindall, R.; Bridgeman, J.; Carliell-Marquet, C. Velocity gradient as a tool to characterise the link between mixing and biogas production in anaerobic waste digesters. *Water Sci. Technol.* **2013**, *67*, 2800–2806.
14. Low, S.C.; Eshtiaghi, N.; Slatter, P.; Baudez, J.-C.; Parthasarathy, R. Mixing characteristics of sludge simulant in a model anaerobic digester. *Bioproc. Biosyst. Eng.* **2016**, *39*, 473–483.
15. Wicklein, E.; Batstone, D.J.; Ducoste, J.; Laurent, J.; Griborio, A.; Wicks, J.; Saunders, S.; Samstag, R.; Potier, O.; Nopens, I. Good modelling practice in applying computational fluid dynamics for WWTP modelling. *Water Sci. Tech.* **2016**, *73*, 969–982.
16. ANSYS. *Fluent 19.2 Theory Guide*; ANSYS, Inc.: Canonsburg, PA, USA, 2018.
17. Maluta, F.; Paglianti, A.; Montante, G. Modelling of biohydrogen production in stirred fermenters by Computational Fluid Dynamics. *Process Saf. Environ. Protect.* **2019**, *125*, 342–357.
18. Dapelo, D.; Bridgeman, J. A CFD strategy to retrofit an anaerobic digester to improve mixing performance in wastewater treatment. *Water Sci. Technol.* **2020**, *81*, 1646–1657.
19. Tobo, Y.M.; Rehman, U.; Bartacek, J.; Nopens, I. Partial integration of ADM1 into CFD: Understanding the impact of diffusion on anaerobic digestion mixing. *Water Sci. Technol.* **2020**, *81*(8), 1658–1667.
20. Zhang, Y.; Yu, G.; Yu, L.; Siddhu, M.A.H.; Gao, M.; Abdeltawab, A.A.; Al-Deyab, S.S.; Chen, X. Computational fluid dynamics study on mixing mode and power consumption in anaerobic mono-and co-digestion. *Bioresour. Technol.* **2016**, *203*, 166–172.
21. Bridgeman, J. Computational fluid dynamics modelling of sewage sludge mixing in an anaerobic digester. *Adv. Eng. Softw.* **2012**, *44*, 54–62.
22. Saini, A.K.; Paritosh, K.; Singh, A.K.; Vivekanand, V. CFD approach for pumped-recirculation mixing strategy in wastewater treatment: Minimizing power consumption, enhancing resource recovery in commercial anaerobic digester. *J. Water Process Eng.* **2020**, *40*, 101777.
23. Dapelo, D.; Alberini, F.; Bridgeman, J. Euler-Lagrange CFD modelling of unconfined gas mixing in anaerobic digestion. *Water Res.* **2015**, *85*, 497–511.
24. López-Jiménez, P.A.; Escudero-González, J.; Martínez, T.M.; Montañana, V.F.; Gualtieri, C. Application of CFD methods to an anaerobic digester: The case of Ontinyent WWTP, Valencia, Spain. *J. Water Process Eng.* **2015**, *7*, 131–140.
25. Meroney, R.N.; Sheker, R.E. CFD simulation of vertical linear motion mixing in anaerobic digester tanks. *Water Environ. Res.* **2014**, *86*, 816–827.
26. Meister, M.; Rezavand, M.; Ebner, C.; Pümpel, T.; Rauch, W. Mixing non-Newtonian flows in anaerobic digesters by impellers and pumped recirculation. *Adv. Eng. Softw.* **2018**, *115*, 194–203.
27. Low, S.C.; Eshtiaghi, N.; Shu, L.; Parthasarathy, R. Flow patterns in the mixing of sludge simulant with jet recirculation system. *Process Saf. Environ. Protect.* **2017**, *112*, 209–221.

28. Hernandez-Aguilar, E.; Alvarado-Lassman, A.; Osorio-Mirón, A.; Méndez-Contreras, J.M. Development of energy efficient mixing strategies in egg-shaped anaerobic reactors through 3D CFD simulation. *J. Environ. Sci. Health A* **2016**, *51*, 536–543.
29. EYS GmbH. Available online: <https://www.eyes-gmbh.de/> (accessed on June 9 2021).
30. Wu, B. CFD simulation of mixing in egg-shaped anaerobic digesters. *Water Res.* **2010**, *44*, 1507–1519.
31. Jamshidzadeh, M.; Kazemzadeh, A.; Ein-Mozaffari, F.; Lohi, A. Analysis of power consumption for gas dispersion in non-Newtonian fluids with a coaxial mixer: New correlations for Reynolds and power numbers. *Chem. Eng. J.* **2020**, *401*, 126002.
32. Li, J.; Deng, B.; Zhang, B.; Shen, X.; Kim, C.N. CFD simulation of an unbaffled stirred tank reactor driven by a magnetic rod: Assessment of turbulence models. *Water Sci. Technol.* **2015**, *72*, 1308–1318.
33. Gao, H.; Stenstrom, M. Evaluation of three turbulence models in predicting the steady state hydrodynamics of a secondary sedimentation tank. *Water Res.* **2018**, *143*, 445–456.
34. Orszag, S.A. Renormalisation group modelling and turbulence simulations. Proceedings of the International Conference on Near Wall Turbulent Flows, Tempe, AZ, Netherlands (1993), pp. 1031-1046.
35. Barrio, R.; Blanco, E.; Fernández, J.; Galdo, M. The use of computational fluid dynamics to estimate fluid residence time and flow hydrodynamics in open digesters of wastewater treatment plants: A case study. *Desalination Water Treat.* **2015**, *53*, 2613–2622.
36. White, F.M. Fluid mechanics. 5th Ed. McGraw-Hill Book Company: Boston, MA, USA, 2003.
37. Hurtado, F.; Kaiser, A.; Zamora, B. Fluid dynamic analysis of a continuous stirred tank reactor for technical optimization of wastewater digestion. *Water Res.* **2015**, *71*, 282–293.
38. Achkari-Begdouri, A.; Goodrich, P.R. Rheological properties of Moroccan dairy cattle manure. *Bioresour. Technol.* **1992**, *40*, 149–156.
39. Hoseini, S.; Najafi, G.; Ghobadian, B.; Akbarzadeh, A. Impeller shape-optimization of stirred-tank reactor: CFD and fluid structure interaction analyses. *Chem. Eng. J.* **2020**, *413*, 127497.
40. Celik, I.B.; Ghia, U.; Roache, P.J.; Freitas, C.J. Procedure for estimation and reporting of uncertainty due to discretization in CFD applications. *J. Fluid. Eng. T. ASME* **2008**, *130*(7), 078001.
41. Vesvikar, M.S.; Al-Dahhan, M. Flow pattern visualization in a mimic anaerobic digester using CFD. *Biotechnol. Bioeng.* **2005**, *89*, 719–732.
42. Zhang, D. Optimize sedimentation tank and lab flocculation unit by CFD. Norwegian University of Life Sciences: As, Norway, 2014.
43. Latha, K.; Velraj, R.; Shanmugam, P.; Sivanesan, S. Mixing strategies of high solids anaerobic co-digestion using food waste with sewage sludge for enhanced biogas production. *J. Clean. Prod.* **2019**, *210*, 388–400.